

## Article

# Vibration Characteristics of Concrete Pump Trucks with Multiple Postures and Multiple Conditions Based on the Secondary Development of HyperWorks

Yafeng Ren <sup>1,\*</sup> , Weifeng Yang <sup>1</sup>, Xiaohui Sun <sup>1</sup>, Jinning Zhi <sup>1</sup>, Jie Li <sup>1</sup> and Haiwei Wang <sup>2</sup><sup>1</sup> School of Mechanical Engineering, Taiyuan University of Science and Technology, Taiyuan 030024, China<sup>2</sup> Shaanxi Engineering Laboratory for Transmissions and Controls, Northwestern Polytechnical University, Xi'an 710072, China

\* Correspondence: renyafeng@tyust.edu.cn

**Abstract:** Due to the excitation generated by the periodically alternate pumping of dual-hydraulic cylinders, vibration of concrete pump trucks (CPT) occurs. Excessive boom vibration will seriously affect the service life and operation safety of CPT. At the same time, the long boom structure of a CPT makes it very sensitive to the posture and pumping conditions, which directly affect the vibration characteristics of CPT in different postures and different working conditions. This paper establishes a finite element model of a type of CPT. Through force analysis of concrete in the straight pipe and elbow pipe during the pumping and reversing stages, an excitation model of the conveying pipe is established. Based on the secondary development of HyperWorks, a finite element model of CPT with multiple postures is built, and the dynamic response under multiple conditions is analyzed. Finally, the accuracy of the finite element model of CPT and the excitation model of the conveying pipe is verified by experiment.

**Keywords:** concrete pump truck; finite element model; boom posture; secondary development; dynamic response analysis



**Citation:** Ren, Y.; Yang, W.; Sun, X.; Zhi, J.; Li, J.; Wang, H. Vibration Characteristics of Concrete Pump Trucks with Multiple Postures and Multiple Conditions Based on the Secondary Development of HyperWorks. *Processes* **2023**, *11*, 1483. <https://doi.org/10.3390/pr11051483>

Academic Editors: Lijian Shi, Kan Kan, Fan Yang, Fangping Tang and Wenjie Wang

Received: 5 April 2023  
Revised: 8 May 2023  
Accepted: 11 May 2023  
Published: 13 May 2023



**Copyright:** © 2023 by the authors. Licensee MDPI, Basel, Switzerland. This article is an open access article distributed under the terms and conditions of the Creative Commons Attribution (CC BY) license (<https://creativecommons.org/licenses/by/4.0/>).

## 1. Introduction

Concrete pump trucks (CPT) are widely used in the construction of residential buildings, bridges, roads and other infrastructure by virtue of their high pouring efficiency, flexibility and safety. However, the impact caused by reversal of the pumping cylinders and the unsteady flow of concrete will induce boom vibration of CPT. Excessive vibration will seriously affect the service life of CPT and the safety of the operator [1]. At the same time, due to the special structure of a long boom system, the vibration is extremely sensitive to the posture and pumping conditions of the boom. Therefore, the dynamic response characteristics of CPT vary with working conditions, which requires dynamic response analysis of CPT under multiple postures and multiple conditions.

At present, research on CPT vibration mainly focuses on concrete flow, vibration mod, vibration response, active control, passive control and real-time boom vibration monitoring. Details of the research are as follows.

Unsteady concrete flow is the main excitation source. In order to study boom vibration, many scholars use CFD, DEM and other fluid simulation software to study the flow properties of concrete in its conveying pipe, so as to obtain the impact force of concrete on the pipe wall. Jiang [2] simulated the flow condition of concrete in its conveying pipe by using CFD-DEM and interior-point algorithm techniques. Aiming at addressing problems such as excessive pumping pressure and even pipe wall rupture caused by the friction of particles on the pipe wall during the flow process, they optimized the conveying pipe to minimize pressure loss during pumping. After optimization, pressure loss is reduced, the particle distribution in the pipeline is more concentrated, and the particle movement

speed is increased. Chen [3] used the combination of smooth particle hydrodynamics and the discrete elements method to simulate and analyze the pumping process of concrete. Finally, the accuracy of the model was verified by experiments. Fan [4] established a hydraulic system of CPT by AMESim software, and obtained dynamic characteristic curves of hydraulic cylinder velocity and displacement at specific conditions by simulation. The relationship between the buffer position and buffer effect was studied by simulating and comparing the hydraulic system with different buffer positions. Ning [5] established a model of a hydraulic system of a pump truck by means of the power linkage chart method, and conducted simulation analysis using Matlab to study the impact of reversing shock in the pumping system and shock due to pushing load.

When the pumping excitation is close to the natural frequency of CPT, it will induce resonance and aggravate boom vibration. Therefore, it is necessary to analyze the modal property of CPT. Zhou [6] identified four dangerous working conditions of CPT, and put forward suggestions to avoid resonance through modal analysis. Mao [7] analyzed the modal analysis of a CPT boom based on natural frequency and modal shape and proposed advice for vibration reduction of CPT.

Excessive vibration at the end boom will cause great harm to CPT. Ren [8] established a model between rigid and flexible dynamics for booms, studied the vibration displacement of the end boom and the first boom hydraulic cylinder force under four common working conditions, and finally verified the accuracy of the established simulation model through tests. Tang [9] studied the dynamic characteristics of the boom system by establishing three dynamic models. By comparing their simulation results with their test results, they found that large-range motion and small flexible deformation should be considered in the study of a boom's dynamic characteristics.

Active control provides an effective means to reduce the vibration of CPT. For example, vibration reduction of a boom can be realized by controlling the stretching of the hydraulic cylinder. Dai [10] analyzed the motion of a boom and hydraulic cylinder through multi-body dynamics, and established a dynamic equation of the boom system combined with PD control theory. Sun [11] proposed closed-loop detection as well as an open-loop control strategy for boom vibration. The angle value collected by the sensors was processed by filtering and curve fitting to reduce the interference of vibration. Finally, the effectiveness of the proposed method was verified by simulation. Cazzulani [12] proposed an active modal TMD control logic for vibration suppression, and verified the superiority of the proposed control logic through numerical simulations of a finite element linear model. Liu [13] proposed an active strategy of vibration suppression based on the modal method, and finally verified the effectiveness of the proposed strategy by experiment.

Passive control such as parameter optimization is another way to reduce vibration. In order to reduce the weight of CPT, Lee [14] used carbon-fiber-reinforced plastic (CFRP) in the structural design of an end boom. Through design evaluation of the boom, the effectiveness of the material applied to the boom structure was verified. Wang [15] optimized the problem of piston striking and insufficient pumping of the pump truck by establishing an optimization model of concrete pumping displacement control.

Real-time monitoring of boom vibration can protect CPT from excessive vibration for a long time. Shen [16] realized real-time measurement of boom vibration through the function of powerful video processing using Matlab. Their experimental results show that the error of this method is small, which verifies its feasibility.

Conventional finite element modeling faces the tedious task of repetitive modeling for multiple poses and multiple working conditions. The secondary development of finite element software can overcome this problem. There is relatively little research on the secondary development of pump truck vibration, and research in other fields is as follows. Lombroni [17] conducted secondary development for the electro-magnetic behavior analysis of plasma when it was vertically displaced in a vacuum chamber through ANSYS software and APDL language. Demircioğlu [18] adopted ANSYS APDL to conduct modal analysis for curved asymmetric sandwich structures with different curvature angles, and

studied the influence of asymmetry and curvature angle on free vibration of sandwich structures. In order to study the influence of different loads on the structural strength and reliability of an offshore derrick, Tan [19] adopted ANSYS APDL language for secondary development and established a strength numerical model of JJ315/45-K. Combined with Python, the stress strength and reliability of the offshore derrick were simulated, and the effects of different loads were analyzed. Ivanova [20] extended augmented reality technology using Tcl/Tk language and Vuforia SDK.

In this paper, the relationship between the stroke of the hydraulic cylinder and the relative angle between adjacent booms under different boom postures will be deduced, which lays a foundation for the automatic adjustment of different postures. At the same time, force analysis of concrete pumping in straight pipes and elbow pipes during the pumping and reversing stages will be deduced to provide a theoretical basis for excitation modeling. Using HyperWorks software, automatic adjustment of the boom posture and automatic dynamic analysis will be developed, and dynamic response analysis of CPT under multiple postures and multiple conditions will be carried out. Finally, the accuracy of the CPT finite element model will be verified by experiment.

## 2. Finite Element Modeling and Boom Posture Transformation

### 2.1. Finite Element Modeling

Due to the complex structure of CPT, it is necessary to simplify, rebuild or clean some parts and geometric features. HyperWorks software is used to establish a finite element model of CPT. The finite element model includes a middle surface unit, a solid unit, a mass unit, a welding unit, and a joint model. Comprehensively considering calculation accuracy and time, a CQUAD4 shell element with a size of 20 mm is used to build the boom system, subframe, rotary turntable, and legs. A CHEXA hexahedron element is used to simulate structures such as the pad, clamp, and bar cavity, which can obtain higher computational accuracy with fewer elements. A WELD element is used to simulate the welding relationship between adjacent panels. A rotational joint element is used to consider the rotation relationship between the axis pin and the connecting rod. A CBUSH spring unit and CONM mass unit are used to simulate the hydraulic oil and rod free cavity of the cylinder. An equivalent density is used for the conveying pipes to reflect the weight of concrete.

Finite element models of the horizontal posture, small-arched posture, and big-arched posture of CPT are shown in Figure 1. The node number of the finite element model is about 1.45 million, and the element number is about 2.19 million. The material parameters of the finite element model of CPT are shown in Table 1.

**Table 1.** Material parameters of the whole vehicle model.

Material	Density (kg/m <sup>3</sup> )	Elastic Modulus (MPa)	Poisson's Ratio
Alloy steel	$7.85 \times 10^3$	$2.1 \times 10^5$	0.300
Rubber pad	$1.63 \times 10^3$	22.6	0.495
Conveyor tube	$7.85 \times 10^3$	$2.1 \times 10^5$	0.300
Pipe hoop rubber sleeve	$1.63 \times 10^3$	10.0	0.495

### 2.2. Geometric Relationship of Booms under Different Postures

The boom system of CPT is a group of spatial structures with multiple freedoms, similar to robots [21]. Therefore, relevant robot theories can be used to study and analyze the kinematics of CPT booms [22,23]. For the CPT studied in this paper, the connection relationship between the booms is a complex multi-link mechanism, which is shown in Figure 2. Points A, B, and E denote the hinge points at the connection of the booms; point D is the hinge point of the connection between the hydraulic cylinder and the boom; point F is the hinge point of the connection between the boom and connecting rod FI; point G is the hinge point of the connection between connecting rod GIH and the boom; point H is

the hinge point of the connection between the hydraulic cylinder and connecting rod GIH; and point I is the hinge point between connecting rod FI and connecting rod GIH.

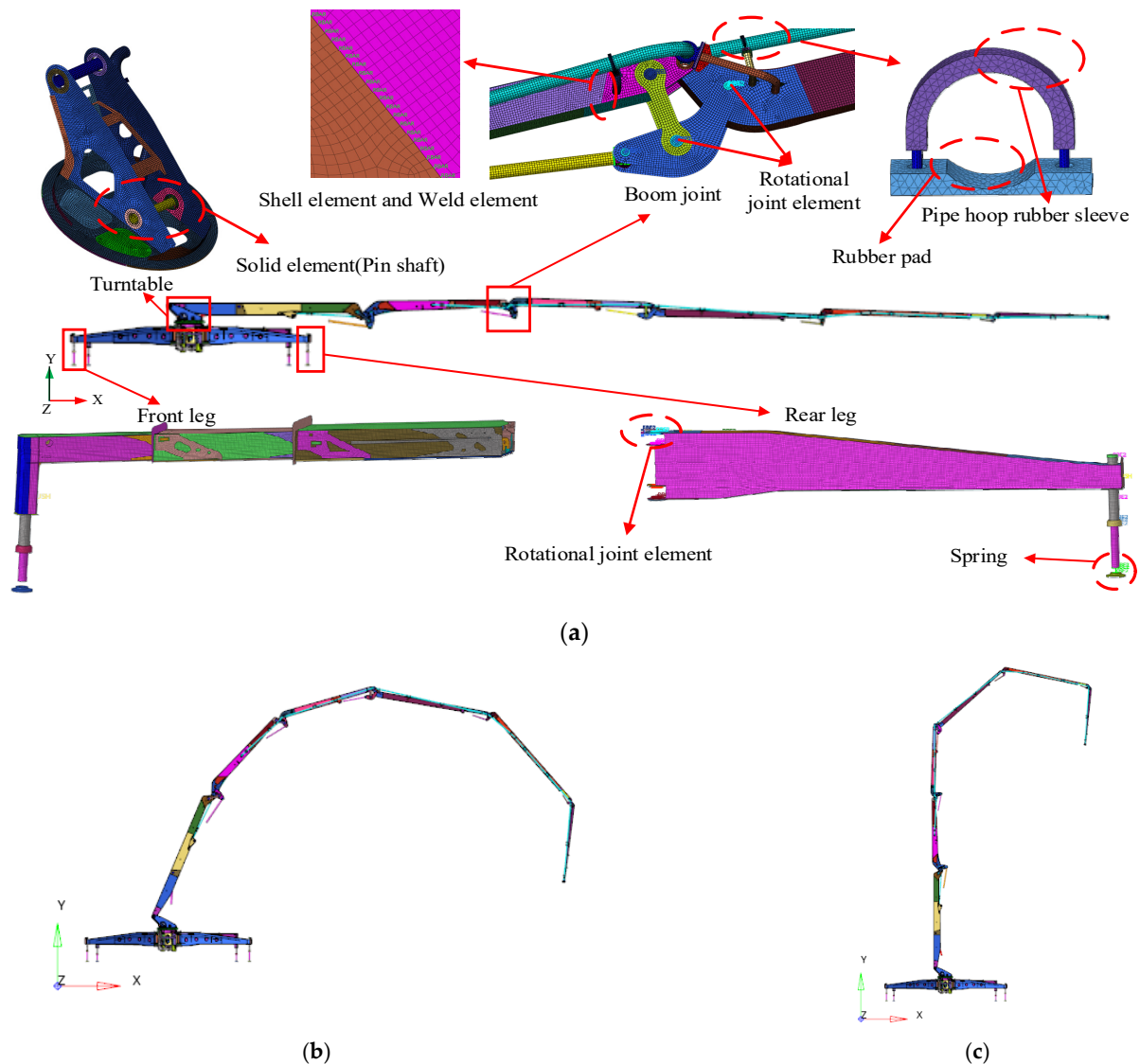


**Figure 1.** The finite element models of CPT. (a) Horizontal posture; (b) big-arched posture; (c) small-arched posture.

Assuming that the length of the hydraulic cylinder stroke ( $L_{DH}$ ) is known and the angle between the boom is unknown ( $\angle BEA$  is in Figure 2), the derivation and solution process can be written as:

$$\varphi = \pi + \varphi_1 \quad (1)$$

where  $\varphi_1$  is the angle between the extension line of  $BE$  and  $EA$ , which is positive when point  $A$  is above  $BE$ , otherwise it is negative.

$$\angle FEG = \pi - \varphi_1 - \angle BEF - \angle GEA \quad (2)$$

where both  $\angle BEF$  and  $\angle GEA$  are structural angles of the boom and have constant values.

In triangle  $\triangle FEG$ :

$$L_{FG} = \sqrt{L_{EF}^2 + L_{EG}^2 - 2 \times L_{EF} \times L_{EG} \times \cos \angle FEG} \quad (3)$$

$$\angle EGF = \arccos \frac{L_{FG}^2 + L_{EG}^2 - L_{EF}^2}{2 \times L_{FG} \times L_{EG}} \quad (4)$$

where  $L_{FG}$  is the distance between hinged point  $F$  and point  $D$ ;  $L_{EF}$  is the distance between point  $E$  and point  $F$ , and is a constant value; and  $L_{EG}$  is the distance between point  $E$  and point  $G$ , and has constant value.

In triangle  $\triangle FIG$ :

$$\angle IGF = \arccos \frac{L_{FG}^2 + L_{GI}^2 - L_{FI}^2}{2 \times L_{FG} \times L_{GI}} \quad (5)$$

where  $L_{GI}$  is the distance between point  $G$  and the point  $I$ , and is a constant value.  $L_{FI}$  is the distance between points  $F$  and  $I$ , i.e., the length of connecting rod  $FI$ .

Based on geometric relationships, the following equation can be derived:

$$\angle EGH = \angle IGF - \angle EGF + \angle IGH \quad (6)$$

where  $\angle IGH$  is the structural angle of the connecting rod  $GIH$ , which has a constant value.

In triangle  $\triangle HEG$ :

$$L_{HE} = \sqrt{L_{HG}^2 + L_{EG}^2 - 2 \cdot L_{HG} \cdot L_{EG} \cdot \cos \angle EGH} \quad (7)$$

$$\angle HEG = \arccos \frac{L_{HE}^2 + L_{EG}^2 - L_{HG}^2}{2 \times L_{HE} \times L_{EG}} \quad (8)$$

where  $L_{HG}$  is the distance between point  $G$  and point  $H$ , and is a constant value.

In triangle  $\triangle DEH$ :

$$\angle DEH = \arccos \frac{L_{DE}^2 + L_{HE}^2 - L_{DH}^2}{2 \times L_{DE} \times L_{HE}} \quad (9)$$

where  $L_{DE}$  is the distance between point  $D$  and point  $E$ , and is a constant value;  $L_{DH}$  is the distance between point  $D$  and point  $H$  which is the length of the hydraulic cylinder stroke, and is a determined value.

$\angle FEG$ ,  $\angle DEF$ ,  $\angle DEH$ , and  $\angle HEG$  have the following geometric relationship:

$$2\pi - \angle FEG = \angle DEF + \angle DEH + \angle HEG \quad (10)$$

where  $\angle DEF$  is the angle formed by points  $D$ ,  $E$ , and  $F$ , and is a constant value.

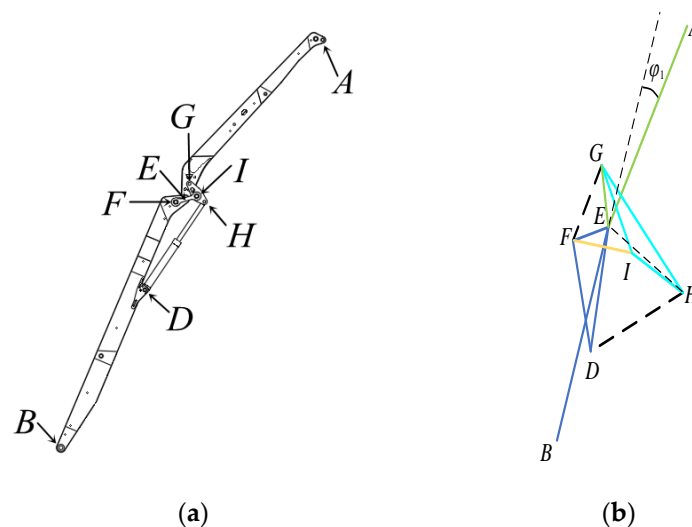


**Figure 2.** The connection relationship of the boom system. (a) Schematic diagram; (b) geometric relations.

From Equation (1) to Equation (10), the relative angle between the boom,  $\varphi$ , will be obtained according to the stroke of the hydraulic cylinder,  $L_{DH}$ . Since most of the connections of the CPT boom have such relationships, to simplify, this paper only lists the derivation process. The relationship between booms is complex and nonlinear, and the relative angle of the boom and cylinder stroke cannot be obtained directly, so Matlab software is adopted to numerically solve this problem.

### 3. Excitation Modeling of the Conveying Pipe

The Bingham model [24] is generally used to describe the flow behavior of concrete. The Bingham model has a critical yield stress, and fluid will flow when the shear stress is greater than the yield stress. Thereafter, the shear strain rate of the fluid is proportional to the shear stress, and its rheological equation can be expressed as:

$$\tau = \tau_0 + \eta\dot{\gamma} \quad (11)$$

where  $\tau$  is the shear stress on the fluid,  $\tau_0$  is the fluid yield strength,  $\eta$  is the fluid viscosity coefficient, and  $\dot{\gamma}$  is the fluid shear strain rate.

When concrete is pumped, a layer of cement mortar along the wall of the pipe will be formed to wrap the concrete. The pumping concrete is assumed to be in a similar form as solid plug flow, maintaining velocity and with pressure not changing with the radius in the same cross-section. The governing equations of its flow in the conveying pipe are the continuity equation and momentum conservation equation, as follows.

The continuity equation can be written as:

$$\rho \frac{dv}{dt} = -\Delta p + \Delta \cdot \tau + \rho g \quad (12)$$

The momentum conservation equation can be expressed as:

$$\frac{\partial(\rho v)}{\partial t} + \text{div}(\rho v v) - \rho F - \text{div} P = 0 \quad (13)$$

where  $p$  is the static pressure of the fluid on each element,  $\rho$  is the density of the fluid,  $\tau$  is the shear stress,  $v$  is the velocity vector of the element,  $g$  is the acceleration of gravity, and  $F$  is the mass force per unit mass of fluid.

The CPT uses two hydraulic cylinders to pump the concrete alternately, so the concrete flows in the conveying pipe during the pumping and reversing stages. Suppose there is friction between the concrete inside the pipe and the surface in contact with the inner wall of the pipe, and there is no friction inside the concrete. The conveying pipe of the CPT is divided into alternately arranged straight pipes and elbow pipes, as shown in Figure 3.

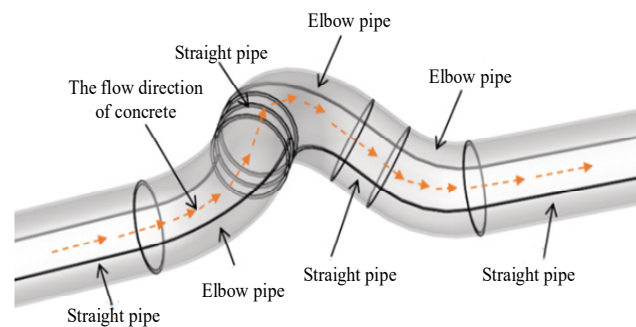


**Figure 3.** The arrangement form of conveying pipes.

#### 3.1. Pumping Stage

Force analysis of concrete in the straight pipe during the pumping stage is shown in Figure 4, and the angle between the direction of gravity and velocity is  $\alpha$ .

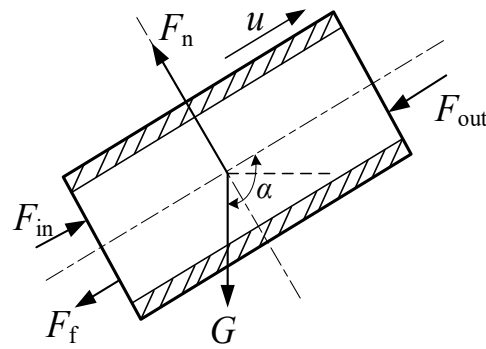


Figure 4. Force analysis diagram of straight pipe in pumping stage.

According to the direction of concrete flow, an equilibrium equation can be established:

$$F_{in} - F_{out} - F_f + G \cos \alpha = ma \tag{14}$$

where  $F_{in}$  is the inlet force of the conveying pipe (N),  $F_{out}$  is the outlet force of the conveying pipe (N),  $F_f$  is the friction force between the concrete and the conveying pipe (N),  $F_n$  is the normal binding force of the concrete wall (N),  $u$  is the velocity of the concrete (m/s),  $G$  is concrete gravity (N),  $m$  is the mass of concrete (kg), and  $a$  is the acceleration of the concrete (m/s<sup>2</sup>).

According to Equation (4), the following equation can be obtained:

$$(p_{in} - p_{out})\pi r^2 - 2\pi r L \left( K_1 + K_2 \frac{V}{\pi r^2} \right) + \rho \pi r^2 (g \cdot L) = \rho L \cdot \frac{dV}{dt} \tag{15}$$

where  $p_{in}$  is the inlet pressure of the conveying pipe (Pa),  $p_{out}$  is the outlet pressure of the conveying pipe (Pa),  $r$  is the radius of the conveying pipe (m),  $L$  is the equivalent length of the conveying pipe (m),  $K_1$  is the adhesion coefficient (Pa),  $K_2$  is the velocity coefficient Pa/(m/s),  $\rho$  is the density of concrete (kg/m<sup>3</sup>),  $g$  is the acceleration of gravity (m/s<sup>2</sup>), and  $V$  is the volume velocity of concrete (m<sup>3</sup>).

Force analysis of the concrete in the elbow pipe during the pumping stage is shown in Figure 5.

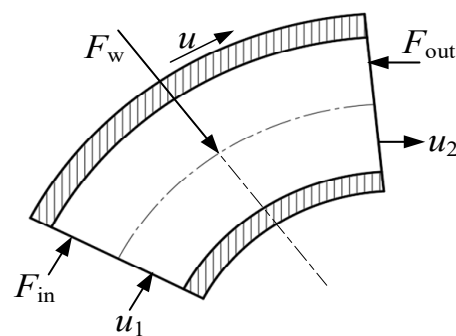


Figure 5. Force analysis diagram of elbow pipe in pumping stage.

Because the length of elbow pipe is relatively small compared with the straight one, the friction between the concrete and pipe wall and the action of gravity on concrete are ignored. In the pumping stage, pressure loss is ignored, and the equation of force balance can be written as:

$$F_{in} = F_{out}; p_{in} = p_{out} \tag{16}$$

The force at the joint of any straight pipe and elbow pipe meets:

$$F_{in}^{i+1} = F_{out}^i; \text{ that is } p_{in}^{i+1} \pi r_{i+1}^2 = p_{out}^i \pi r_i^2 \tag{17}$$

For the whole system, through comprehensive calculation of the force balance equation of each pipe section, one can yield:

$$\begin{aligned} \pi r_i^2 p_{\text{in}} - \pi r_i^2 p_{\text{out}} - \sum_{i=1}^n 2\pi r_i L_i K_1 - \sum_{i=1}^n \frac{2L_i}{r_i} K_2 V \\ + \sum_{i=1}^n \rho \pi r_i^2 (g \cdot L_i) = \sum_{i=1}^n \rho L_i \frac{dV}{dt} \end{aligned} \quad (18)$$

Acceleration is ignored to analyze the quasi-static conditions. The force of concrete in the straight pipe can be expressed as:

$$F_{\text{out}}^i = p_{\text{out}}^i \pi r_i^2 \quad (19)$$

$$F_f^i = 2\pi r_i L_i \left( K_1 + K_2 \frac{V}{\pi r_i^2} \right) \quad (20)$$

The force of concrete in the elbow pipe is formulated as:

$$(F_w^i + F_{\text{in}}^i + F_{\text{out}}^i) \Delta t = m(u_2 - u_1) \frac{V}{\pi r_i^2} \quad (21)$$

where  $F_w$  is the steering force on the concrete in the pumping stage (N) and  $\Delta t$  is the working time of the hydraulic cylinder within the pumping cycle (s).

$$F_w^i = \left( \frac{V^2 \rho}{\pi r_i^2} + F_{\text{in}}^i \right) (u_2 - u_1) \quad (22)$$

### 3.2. Reversing Stage

Force analysis of concrete in the straight pipe in the reversing stage is shown in Figure 6. At this stage, it is assumed that the concrete speed is zero.

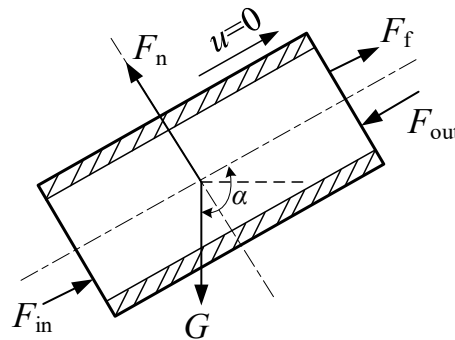


Figure 6. Force analysis diagram of concrete in straight pipe.

By establishing a balance equation along the flow direction of concrete, one can obtain:

$$(p_{\text{in}} - p_{\text{out}}) \pi r^2 + 2\pi r L \left( K_1 + K_2 \frac{V}{\pi r^2} \right) + \rho \pi r^2 (g \cdot L) = 0 \quad (23)$$

The force on the elbow pipe in the reversing stage is similar to that in the pumping stage. The force on the elbow pipe is as follows:

$$p_{\text{in}}^i = p_{\text{out}}^i \quad (24)$$

The force of the straight pipe applied on the concrete is:

$$F_{\text{out}}^i = p_{\text{out}}^i \pi r_i^2 \quad (25)$$

$$F_f^i = -\text{sign}(g \cdot u_i) \cdot \min \{ 2\pi r_i L_i \cdot K_1, \text{abs}[\rho \pi r_i^2 (g \cdot L_i)] \} \quad (26)$$

$$F_{in}^i = F_{out}^i - F_f^i - \rho \pi r_i^2 (g \cdot L_i) \quad (27)$$

The force of the elbow pipe on the concrete is:

$$F_c^i = F_{in}^i (u_2 - u_1) \quad (28)$$

where  $F_c$  is the binding force of concrete in the reversing stage (N).

For Equations (14)–(28), script files are written in the form of Matlab scripts to yield the excitation of each pipe. The action force of concrete on the conveying pipe and that of the conveying pipe on concrete are interaction forces. For the whole system, the above forces can be combined to obtain the impact load of each pipe section. Through the secondary development platform, the excitation results are loaded for automatic dynamic response analysis. The excitation curve under a certain pumping condition is shown in Figure 7. Figure 8a shows the load position of the chassis conveying pipe, and Figure 8b shows the load position of the conveying pipe.

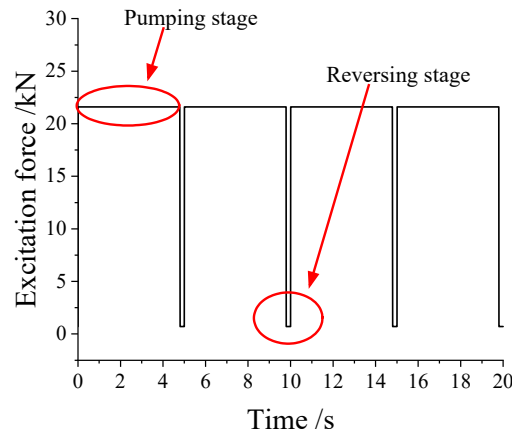


Figure 7. Time history curve of pumping excitation.

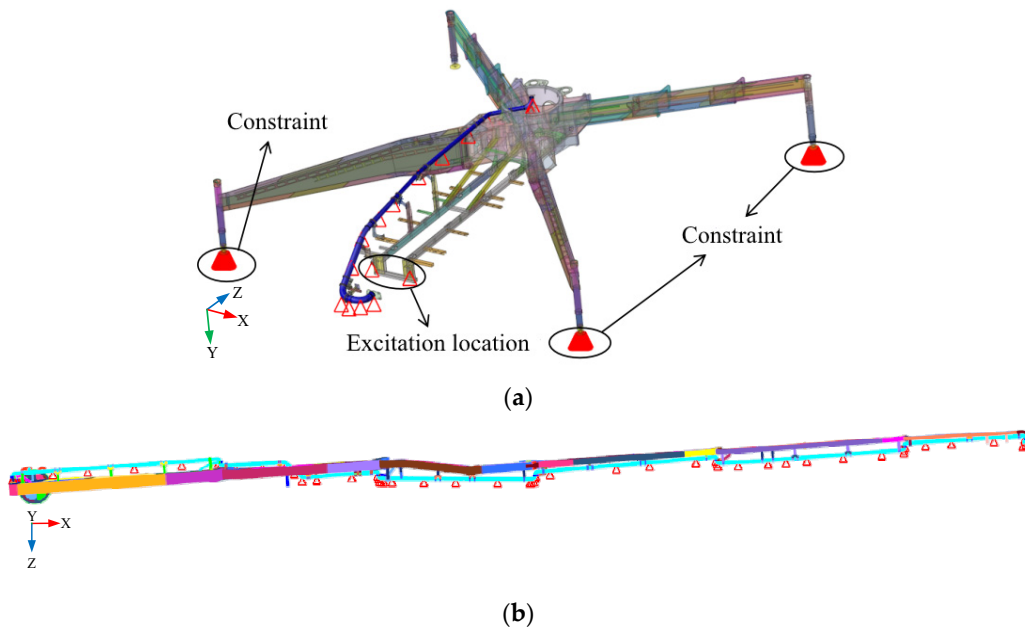


Figure 8. Excitation load position of CPT. (a) Load position of conveying pipe of the chassis; (b) load position of conveying pipe of the boom.

## 4. Secondary Development and Dynamic Response Analysis Based on HyperWorks

### 4.1. Secondary Development Summary of HyperWorks

At present, finite element analysis software is widely used, such as HyperWorks, ANSYS, ABAQUS, and NASTRAN. Due to its complex operation, low efficiency, and excessive dependence on engineers, traditional finite element analysis is gradually failing to meet the needs of enterprise development. To solve these problems, finite element analysis software provides a secondary development environment to facilitate customers to realize automation of the finite element analysis process, greatly shortens the research and development cycle, and improves analysis efficiency [19].

Secondary development of HyperWorks mainly uses Tcl/Tk language and HyperWorks software built-in functions and toolkits. Developers can check the help documentation to discover what these functions do and how to use them.

### 4.2. Working Principle of Secondary Development

In this paper, posture information of CPT is calculated with different parameter data (cylinder stroke or relative angle between booms). Based on the derived posture relationship, a Matlab script is created and called to carry out real-time calculation of the target posture information to complete the calculation of relative parameters. The main process of secondary development is shown in Figure 9, and the specific process is as follows:

1. Input parameters into the platform for automatic adjustment of boom posture. The platform evaluates the parameters input by the user according to the adjustment range of the posture parameters. If the parameters are within the adjustment range of the posture parameters, the next step can be proceeded with. Otherwise, a message is displayed indicating that the parameter is incorrect, and the parameter should be input again.
2. Calculate the target posture parameters using Matlab. According to the parameters input by the user, the automatic adjustment platform of the boom posture calls Matlab to calculate and solve the parameters of the target posture, and the final calculation results are submitted to HyperWorks.
3. HyperWorks performs a change of boom posture according to the posture parameter information. The automatic adjustment platform of the boom posture will obtain the parameter information of CPT under the current posture and submit these parameters to HyperWorks. HyperWorks will compare the information of the current and target postures. After comparison, posture change of the finite element model will be carried out. Then, the operation will be evaluated, and if the change is successful, the subsequent operation can be carried out. Otherwise, it will return to the automatic adjustment platform of the boom posture and prompt the user to redo.
4. Input parameters into the automation analysis platform of dynamic response. Execute relevant settings, including time step, modal damping, modal order, loading of excitation, excitation curve, transient response excitation, superposition of transient excitation, load condition of transient analysis, output nodes, and output solution. The automation dynamic analysis platform evaluates the user's settings, and carries out the next operation if the parameters are set reasonably; otherwise, a message is displayed indicating that the parameter settings are incorrect and need to be redone.
5. Dynamic response analysis. The automation analysis platform of dynamic response will call Optistruct solver to process and analyze the finite element model according to the user's settings. After the solution is completed, a result file will be generated for post-processing analysis.

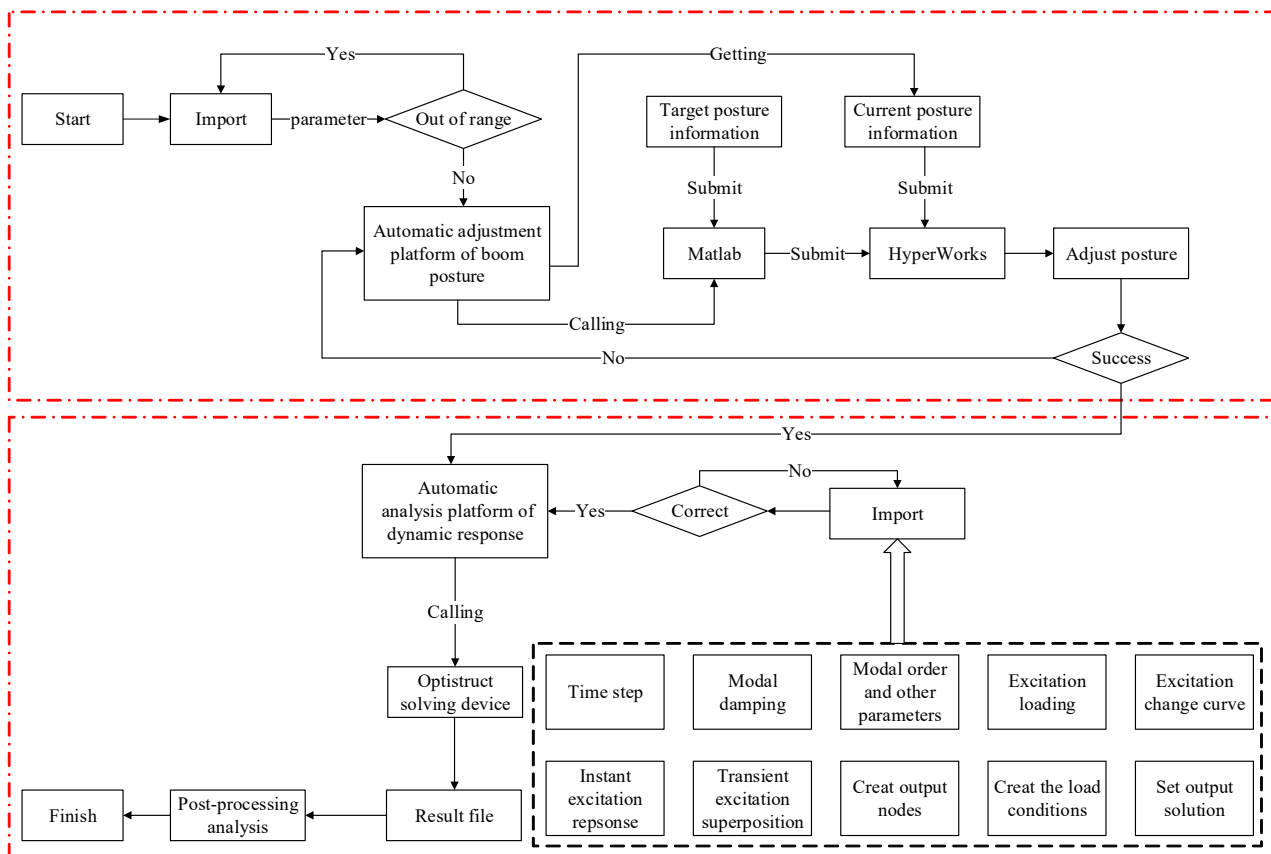


Figure 9. The main process of the secondary development.

#### 4.3. The Secondary Development Platform for Dynamic Response Analysis under Multiple Postures and Multiple Conditions

Based on the above principles of secondary development, the automatic adjustment of the boom posture and automatic dynamic analysis are developed, and the interface of corresponding automatic functions is made by Tk. The interface of the platform for automatic adjustment of boom posture is shown in Figure 10, and the platform for automatic analysis of dynamic response is shown in Figure 11.

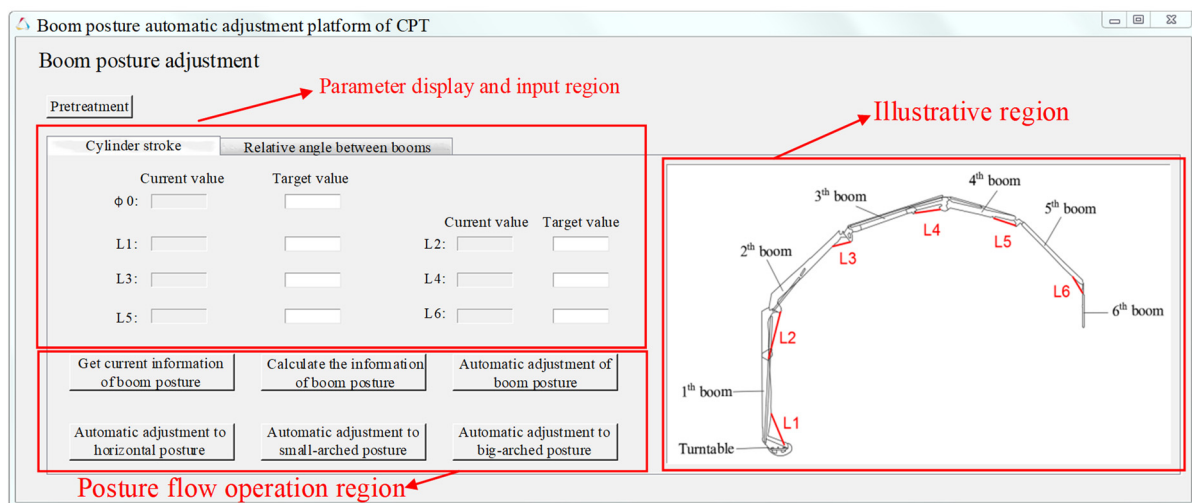
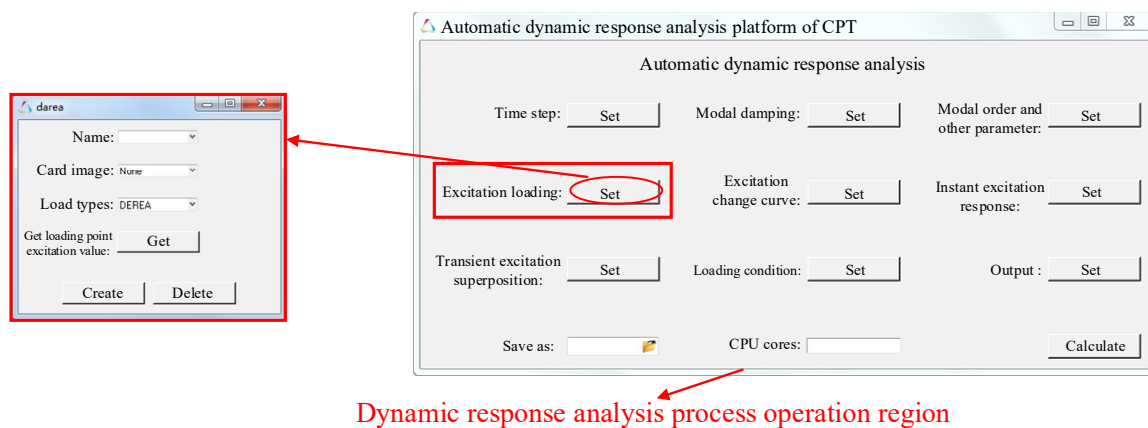


Figure 10. The operating interface of automatic boom posture adjustment platform of CPT.



**Figure 11.** The operation interface of automatic dynamic response analysis platform of CPT.

In Figure 10, the upper-left corner of the interface is the pre-processing operation region of the platform for automatic adjustment of boom posture, which is mainly used to obtain the key position parameters of the boom and to facilitate the subsequent platform to obtain the parameter information. The left side of the interface is the display and input region of the boom posture parameters and the operation region of the posture flow, respectively. The regions of parameter display and input are mainly a display of the current posture information of the boom and the input of the target posture information. The operation region of the posture flow allows users to obtain different posture information, adjust posture, or perform automatic adjustment of three typical postures according to analysis requirements. The right side of the interface is the schematic description region of the boom posture parameters. Users can intuitively understand the meanings of different parameters according to the parameter labels in the schematic diagram.

In Figure 11, the automatic analysis platform of dynamic response includes the operation region of different analysis processes, the storage path of solving files, and the number of CPU cores called in the solving process. The left side of Figure 11 shows the second-level menu for settings in one of the steps of the process of dynamic response analysis. During the settings process, different settings are completed according to the corresponding message in the second-level menu.

#### 4.4. Dynamic Response Analysis of CPT with Multiple Postures and Multiple Conditions

The complex working environment of CPT and the excitation generated by its periodic pumping will lead to excessive vibration at the boom end of CPT, which affects the service life and operation safety of CPT. CPT is very sensitive to the posture of the boom. The vibration characteristics of CPT are very sensitive to the boom posture and working conditions. Therefore, it is necessary to analyze the dynamic response of CPT under different postures and working conditions.

The target posture is adjusted directionally by the automatic adjustment platform of the boom posture. After the adjustment, the target posture of CPT is analyzed by the automatic dynamic analysis platform. The dynamic response under different postures is obtained, and the vibration displacement of the boom end is extracted according to the node number. The vibration displacement data of X, Y, and Z directions are exported in HyperView, and the exported vibration displacement data are processed by Matlab. The rotation angle of the turntable is  $87^\circ$ , the pumping frequency is 0.267 Hz, and the pumping pressure is 7 MPa. The vibration displacement curves of the end boom of CPT in the time domain under horizontal posture are shown in Figure 12a, Figure 12c, and Figure 12e, respectively. Through Fourier transform, vibration displacement curves in the frequency domain in the corresponding direction can be obtained. The vibration displacement curves in the frequency domain are shown in Figure 12b, Figure 12d, and Figure 12f, respectively.

To facilitate the analysis of the correspondence between peak frequencies in Figure 12 and the system natural frequencies, the first four order natural frequencies of the whole vehicle obtained by modal analysis under the three typical postures are listed in Table 2.

By analyzing the three curves in Figure 12a,c,e, it can be seen that the steady vibration displacement in the X direction is 0.018 m, that in the Y direction is 0.130 m, and that in the Z direction is 0.220 m. The vibration displacement curve of the frequency domain in the X direction is shown in Figure 12b, which is mainly distributed within 8 Hz. The first peak frequency is 1.6 Hz—that is, 6 times the excitation frequency, which is very close to the 9th natural frequency of CPT (1.66 Hz). The second peak frequency is 1.866 Hz—that is, 7 times the excitation frequency, which is very close to the 11th natural frequency of CPT (1.86 Hz). The third peak frequency is 2.666 Hz—that is, 10 times the excitation frequency, which is very close to the 13th natural frequency of CPT (2.6 Hz). The vibration displacement curve of the frequency domain in Y direction is shown in Figure 12d, which is mainly distributed within 4 Hz, and the first peak frequency is 0.2666 Hz, which is the pumping frequency. The second peak frequency is 0.5333 Hz—that is, twice the frequency of excitation frequency, which is very close to the 3rd natural frequency of CPT (0.54 Hz). The third peak frequency is 1.866 Hz—that is, 8 times the excitation frequency, which is very close to the 11th natural frequency of CPT (1.86 Hz). The vibration displacement curve of the frequency domain in the Z direction is shown in Figure 12f, which is mainly distributed within 4 Hz. The first peak frequency is 0.5333 Hz—that is, twice the frequency of the excitation frequency, which is very close to the third-order natural frequency of CPT (0.54 Hz). The second peak frequency is 2.666 Hz—that is, 10 times the excitation frequency, which is very close to the 13th natural frequency of CPT (2.6 Hz). The third peak frequency is 2.933 Hz—that is, 11 times the excitation frequency.

**Table 2.** The first four order natural frequencies of the CPT under three typical postures.

Order	Horizontal Posture (Hz)	Small-Arched Posture (Hz)	Big-Arched Posture (Hz)
1	0.16	0.18	0.15
2	0.20	0.24	0.20
3	0.54	0.36	0.33
4	0.60	0.39	0.38

Through the analysis of the dynamic response of CPT under three typical postures, different pumping frequencies, and different pumping pressures, the vibration displacements of CPT under different working conditions are shown in Table 3, Table 4, and Table 5, respectively, and a comparison of corresponding vibration displacements is shown in Figure 13. It can be seen from Figure 13 that the vibration in the y direction is the highest and the vibration in the z direction is the lowest under the same attitude and working conditions. The posture, pumping frequency, and pumping pressure have a great influence on the vibration of CPT. Higher pumping pressure can lead to more intense vibrations. The influence of posture and pumping frequency is complex and depends on the structure mode.

**Table 3.** Vibration displacement of the boom end under three typical postures (X direction/m).

Posture of boom	Pumping pressure (MPa)	Pumping frequency (Hz)						
		0.117	0.200	0.233	0.267	0.300	0.350	0.383
Horizontal posture	7	0.024	0.023	0.026	0.018	0.019	0.028	0.016
	10	0.030	0.034	0.028	0.027	0.030	0.042	0.027
Small-arched posture	7	0.190	0.075	0.160	/	/	/	/
	10	0.520	0.170	0.620	0.180	0.110	0.064	0.041
Big-arched posture	7	0.230	0.570	0.160	0.050	0.080	0.040	/
	10	0.480	1.820	0.570	0.260	0.260	0.160	0.200

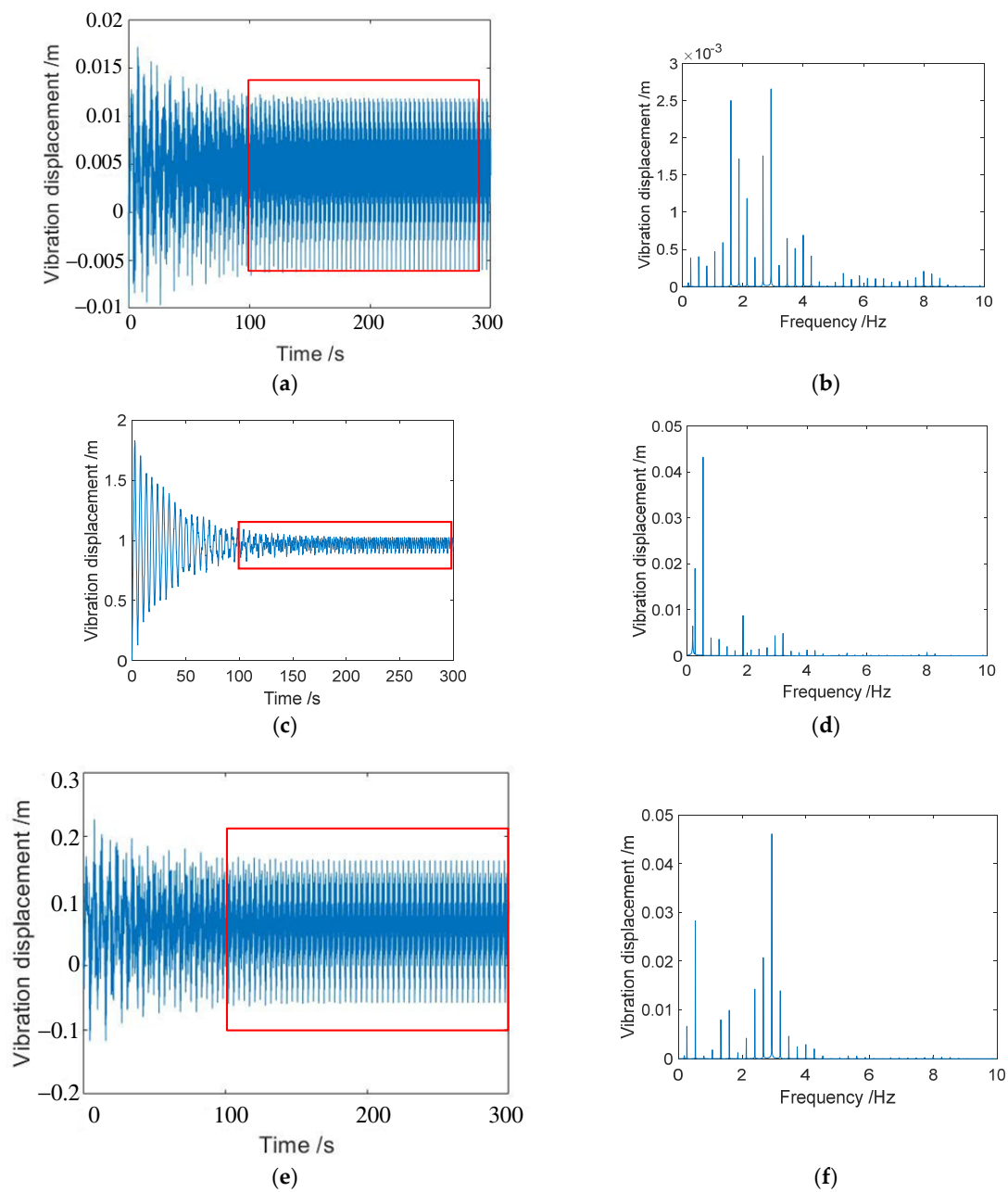


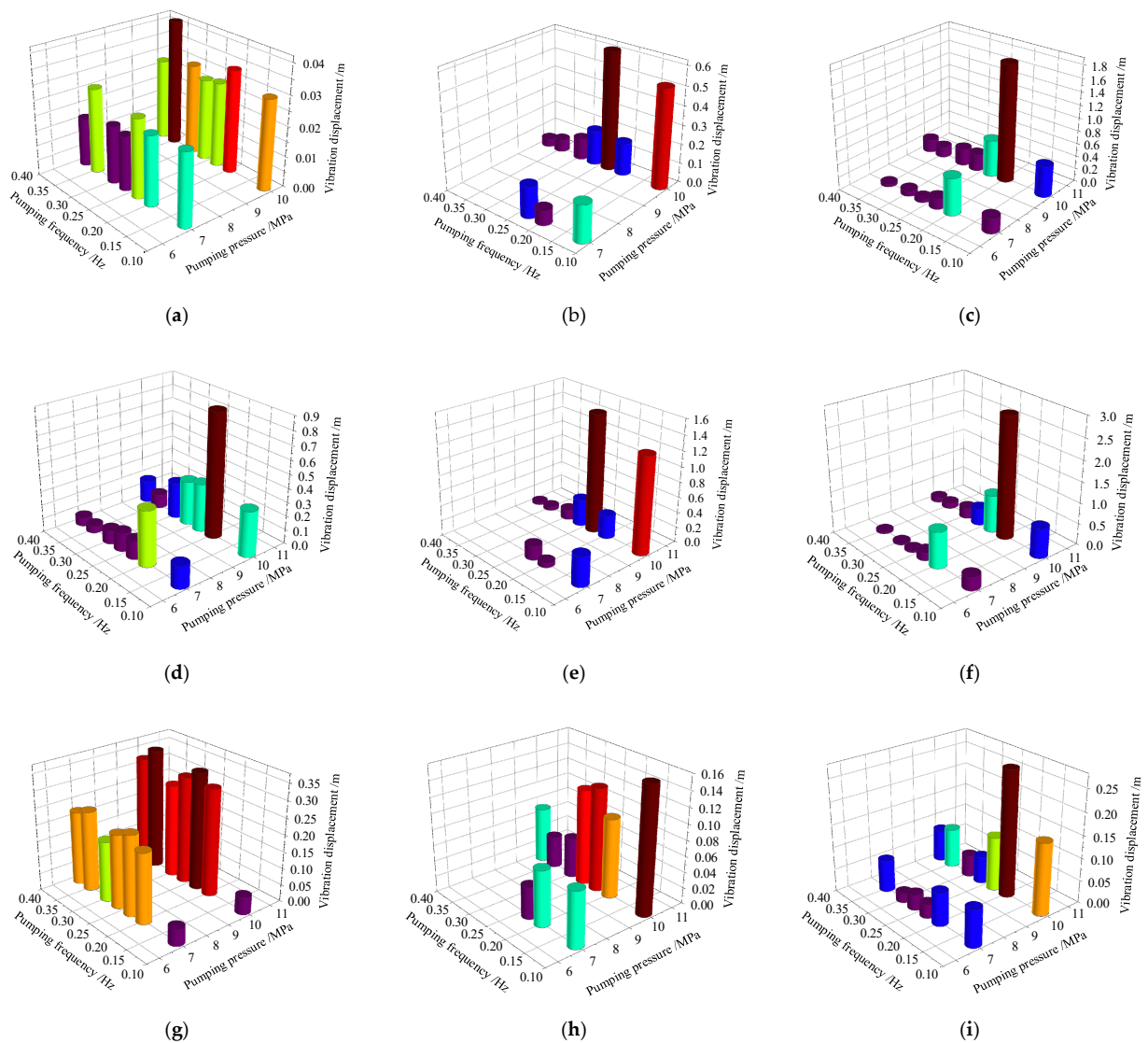
**Figure 12.** The vibration displacement of the boom end. (a) Time-domain displacement diagram (X direction); (b) displacement spectrum diagram (X direction); (c) time-domain displacement diagram (Y direction); (d) displacement spectrum diagram (Y direction); (e) time-domain displacement diagram (Z direction); (f) displacement spectrum diagram (Z direction).

**Table 4.** The vibration displacement of the end boom under the three typical postures (Y direction/m).

Posture of boom	Pumping pressure (MPa)	Pumping frequency (Hz)						
		0.117	0.200	0.233	0.267	0.300	0.350	0.383
Horizontal posture	7	0.160	0.400	0.130	0.130	0.096	0.050	0.060
	10	0.330	0.900	0.350	0.320	0.260	0.100	0.160
Small-arched posture	7	0.390	0.055	0.180	/	/	/	/
	10	1.280	0.300	1.550	0.350	0.130	0.050	0.030
Big-arched posture	7	0.310	0.860	0.190	0.040	0.030	0.040	/
	10	0.710	2.90	0.900	0.400	0.250	0.130	0.110

**Table 5.** The vibration displacement of the end boom under the three typical postures (Z direction/m).

Posture of boom	Pumping pressure (MPa)	Pumping frequency (Hz)						
		0.117	0.200	0.233	0.267	0.300	0.350	0.383
Horizontal posture	7	0.050	0.210	0.240	0.220	0.180	0.240	0.220
	10	0.052	0.320	0.350	0.320	0.280	0.360	0.320
Small-arched posture	7	0.070	0.070	0.040	/	/	/	/
	10	0.160	0.100	0.130	0.120	0.050	0.040	0.070
Big-arched posture	7	0.082	0.073	0.030	0.034	0.020	0.070	/
	10	0.160	0.280	0.120	0.060	0.048	0.088	0.073

**Figure 13.** Vibration displacement under three typical postures. (a) X direction of horizontal posture; (b) X direction of small-arched posture; (c) X direction of big-arched posture; (d) Y direction of horizontal posture; (e) Y direction of small-arched posture; (f) Y direction of big-arched posture; (g) Z direction of horizontal posture; (h) Z direction of small-arched posture; (i) Z direction of big-arched posture.

The vibration in the X direction of the horizontal posture is less than 0.05 m, and the vibration in the Z direction is less than 0.4 m. The maximum vibration in the Y direction occurs at 0.2 Hz pumping frequency, which should be avoided. The vibration of the small-arched posture in the X direction is less than 0.65 m, and the vibration in the Z direction is less than 0.2 m. The maximum vibration in the Y direction is 1.55 m, which occurs at 0.233 Hz pumping frequency, and 10 MPa pumping pressure and should be avoided. The maximum vibration of the big-arched posture in the X direction is 1.82 m at 0.2 Hz and 10 MPa; the maximum vibration in the Y direction is 2.9 m at 0.2 Hz and 10 MPa; and the vibration in the Z direction is less than 0.3 m. Pumping at 0.2 Hz should be avoided for the big-arched posture.

## 5. Experimental Validations

### 5.1. Test Methods and Procedures

Two uniaxial accelerometers were installed at the boom end, and vibration signals were collected using a SoundBook MK2 dynamic vibration meter. The frequency spectrum characteristics of vibration displacement and acceleration at the end boom were obtained through data post-processing.

During the working process of CPT, the posture of the boom was adjusted to an approximately horizontal posture, and the tested surface of the boom was cleaned. Then two uniaxial accelerometers were arranged vertically and laterally at the boom end, and connected with a dynamic vibration meter; to connect the sensor, equipment, and computer, the test parameters of the dynamic vibration meter were set, and pre-test debugging was conducted. The sampling frequency of the dynamic vibration meter was 5 kHz, and the sampling time was determined according to the working condition. After CPT started working and reached a stable pumping state, the dynamic vibration meter was started for measurement. Meanwhile, all test data and engine speed, pumping pressure, and reversing frequency of CPT during operation were recorded, as shown in Table 6. After the test, the data were exported for post-processing and analysis. The test site is shown in Figure 14.

Table 6. Record table of pumping test for CPT.

Project	Pumping Frequency (Hz)	Pumping Capacity (%)	Pumping Pressure (MPa)	Rotation Angle of Turntable (°)	Engine Speed (r/min)	Posture of Boom	Measuring Point Position
1st condition	0.30	44	11.2	−167	1447	Approximately	The end boom
2nd condition	0.27	40	10.0	−171	1362	horizontal	
3rd condition	0.25	38	9.5	−168	1234	posture	

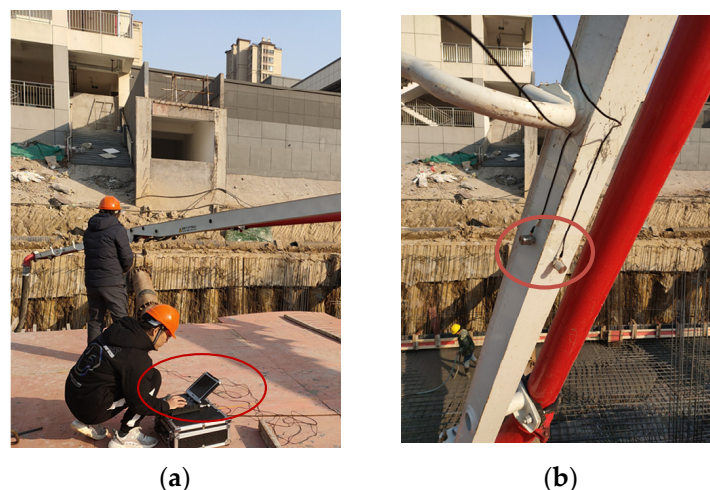
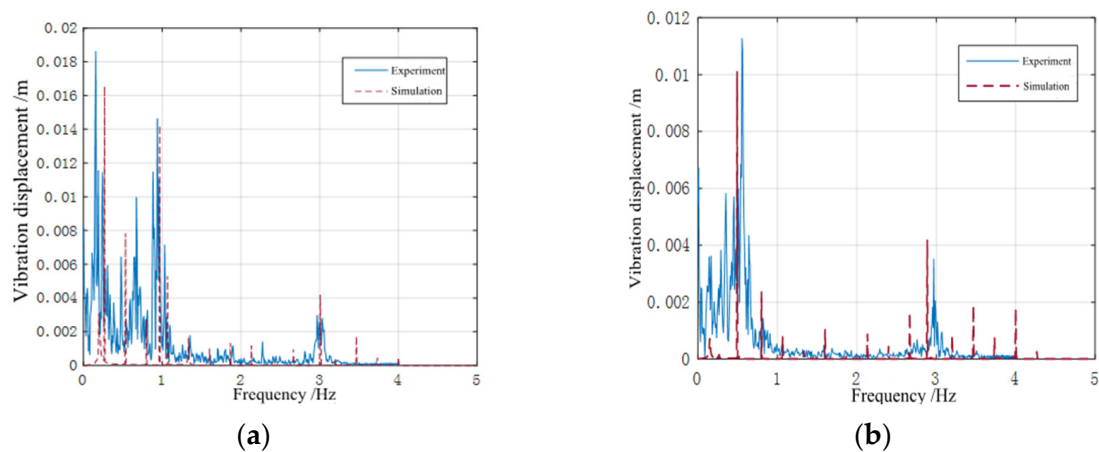


Figure 14. Placement diagram of the real vehicle test. (a) Dynamic vibration meter; (b) acceleration sensor.

### 5.2. Analysis of Test Results

The pumping frequency under the test condition is 3–6/min, which is 0.25–0.30 Hz. The vibration displacement curves of the Y direction and Z direction of the boom end under common working conditions were obtained, and the comparison between the frequency response curves and simulation curves obtained by Fourier transform is shown in Figure 15. The corresponding frequencies of the first five peaks are compared respectively, as shown in Table 7. It can be seen that the difference between the test results and the simulation results is within 20%. The reason for this difference is that the finite element model has been simplified and CPT is subjected to complex external forces such as wind load while working. In addition, the posture of the boom and the pumping conditions were changing from time to time.



**Figure 15.** Comparison of the vibration in the frequency domain. (a) The frequency vibration in the Y direction; (b) the frequency vibration in the Z direction.

**Table 7.** Peak frequency comparison.

Peak Value	1	2	3	4	5
Simulation (Y)	0.193	0.266	0.533	0.80	0.966
Experiment (Y)	0.187	0.242	0.476	0.672	0.938
Difference/%	3.1	9.0	10.7	16.0	2.9
Simulation (Z)	0.146	0.266	0.493	0.526	1.067
Experiment (Z)	0.140	0.289	0.554	0.602	1.055
Difference/%	4.1	8.6	12.4	14.4	1.1

## 6. Conclusions

In this paper, the secondary development of automatic boom posture adjustment and automatic dynamic response analysis based on Hyperworks was carried out with CPT. An excitation model of the conveying pipe was proposed to analyze the dynamic response of CPT under multiple postures and multiple conditions. The main conclusions are as follows:

1. Automatic boom posture adjustment technology can aid kinematics analysis, static strength analysis, and dynamic response analysis of CPT.
2. Automatic dynamic response analysis technology can assist modal analysis, vibration displacement analysis, dynamic strength analysis, and vehicle vibration stability analysis of CPT.
3. By comparing vibration response through experimentation and simulation, it can be seen that the difference between the test value and the simulation value is less than 20%, which verifies the reliability of the analysis method of dynamic response in this paper.

4. Through analysis of the pumping excitation and dynamic response of CPT under multiple conditions, it can be seen that the vibration of CPT is mainly composed of pumping frequency and its low-order harmonic components. According to the test results, it is accurate enough to consider only the first five order harmonics of pumping frequency in the simulation model.
5. Posture, pumping frequency, and pumping pressure have a great influence on the vibration of CPT. Higher pumping pressure can lead to more intense vibrations. The influence of posture and pumping frequency is complex and depends on the structure mode. Through dynamic analysis, the pumping frequency and harmonic components within 4 Hz have a great impact on the vibration characteristics.
6. Future research could focus on the elimination of concrete pumping excitation induced by air injection, dynamic strength of structure analysis, vehicle vibration stability analysis, and low vibration optimization of booms under multiple postures and multiple work conditions.

**Author Contributions:** Conceptualization, Y.R. and J.Z.; methodology, Y.R.; software, W.Y.; validation, J.L. and H.W.; data curation, X.S.; writing—original draft preparation, W.Y.; writing—review and editing, X.S. All authors have read and agreed to the published version of the manuscript.

**Funding:** This research was funded by the Shanxi Basic Research Project (Grant No. 20210302124445, 201901D111245), Shanxi Provincial Science and Technology Platform (201805D121006), and Shanxi Excellent Doctor's Work Award Fund (Grant No. 20202061).

**Data Availability Statement:** The data presented in this study are available on request from the corresponding author.

**Conflicts of Interest:** The authors declare no conflict of interest.

## References

1. Yang, P.; Wang, R.; Shao, Y.H.; Lv, P.M. Dynamic Simulation of Concrete Pump Truck's Boom System Based on Rigid-Flexible Coupling Model. *Appl. Mech. Mater.* **2012**, *246*, 989–993. [[CrossRef](#)]
2. Jiang, S.; Zhang, W.; Chen, X.; Cao, G.; Tan, Y.; Xiao, X.; Liu, S.; Yu, Q.; Tong, Z. CFD-DEM simulation research on optimization of spatial posture of concrete pumping boom based on evaluation of minimum pressure loss. *Powder Technol.* **2022**, *403*, 117365. [[CrossRef](#)]
3. Chen, W.; Wu, W.; Lu, G.; Tian, G. Simulation Analysis of Concrete Pumping Based on Smooth Particle Hydrodynamics and Discrete Elements Method Coupling. *Materials* **2022**, *15*, 4294. [[CrossRef](#)] [[PubMed](#)]
4. Fan, C.G.; Zeng, F.L.; Li, D.H.; Liu, L. Simulation Study of the Hydraulic System of Concrete Pumping Truck Based on AMESim. *Appl. Mech. Mater.* **2012**, *1800*, 1920–1925. [[CrossRef](#)]
5. Ning, Q.W.; Yu, W.H. Pressure Analysis of Hydraulic Pumping System of Concrete Pump. *Adv. Mater. Res.* **2011**, *383–390*, 7543–7549.
6. Zhou, X.X.; Xu, C.L.; Ren, N.N.; Guo, S.J.; Tian, R.L. Modal Analysis of the Boom System of Truck-Mounted Concrete Pump. *Adv. Mater. Res.* **2011**, *403*, 3620–3625. [[CrossRef](#)]
7. Mao, K.L. Modal Analysis of Concrete Pump Truck Boom. *Adv. Mater. Res.* **2014**, *2990*, 148–151. [[CrossRef](#)]
8. Ren, W.; Li, Z.; Bi, Y.; Zhao, S.; Peng, B.; Zhou, L. Modeling and Analysis of Truck Mounted Concrete Pump Boom by Virtual Prototyping. *J. Robot.* **2017**, *2017*, 1–10. [[CrossRef](#)]
9. Tang, H.B.; Ren, W. Research on rigid-flexible coupling dynamic characteristics of boom system in concrete pump truck. *Adv. Mech. Eng.* **2015**, *7*, 1687814015573854. [[CrossRef](#)]
10. Dai, L.; Wang, J.; Zhao, B.; Liu, J. Multi-Body Dynamic PD Control of Concrete Pump Truck Arm System. *Appl. Mech. Mater.* **2009**, *875*, 806–810. [[CrossRef](#)]
11. Sun, X.J.; Ye, H.; Fei, S.M. A closed-loop detection and open-loop control strategy for booms of truck-mounted concrete pump. *Autom. Constr.* **2013**, *31*, 265–273. [[CrossRef](#)]
12. Cazzulani, G.; Ghielmetti, C.; Resta, F.; Ripamonti, F. Vibration control of flexible structures with an Active Modal Tuned Mass Damper. *IFAC Proc. Vol.* **2011**, *44*, 5371–5376. [[CrossRef](#)]
13. Liu, R.; Gao, Y.; Yang, S.; Yang, Y. Vibration Control of the Boom System of Truck-Mounted Concrete Pump Based on Constant-Position Commandless Input Shaping Technique. *Shock Vib.* **2015**, *2015*, 1–9. [[CrossRef](#)]
14. Lee, S.J.; Chung, I.S.; Bae, S.Y. Structural design and analysis of CFRP boom for concrete pump truck. *Mod. Phys. Lett. B* **2019**, *33*, 1940033. [[CrossRef](#)]
15. Wang, A.L.; Shi, Z.Q.; Yuan, C.X.; Hu, Y.Q. Optimal Design of Concrete Pumping Displacement Control. *Adv. Mater. Res.* **2011**, *422*, 238–242. [[CrossRef](#)]

16. Shen, C.; Yi, P.L. Displacement Measuring Method of Flexible Boom Based on MATLAB Video Processing. *Appl. Mech. Mater.* **2014**, *3436*, 432–435.
17. Lombroni, R.; Carusotti, S.; Giorgetti, F.; Scarpari, M.; Buxton, P.; Calabrò, G.; Fanelli, P.; Romanelli, M.; Valdes, E.R.d.V.; Wood, J. Use of MAXFEA-ANSYS tool to study the Electro-Magnetic behaviour of the new ST40 inner vacuum chamber proposal during a plasma VDE. *Fusion Eng. Des.* **2023**, *192*, 113611. [[CrossRef](#)]
18. Demircioğlu, U.; Çakır, M.T. Free vibration analysis of curved asymmetric sandwich structures. *J. Eng. Res.* **2023**, *11*, 100036. [[CrossRef](#)]
19. Tan, Z.; Chen, H.; Wan, F.; Liao, F.; Gao, Y.; Cai, C. Influence of Complex Load on the Strength and Reliability of Offshore Derrick by Using APDL and Python. *Appl. Sci.* **2022**, *12*, 11693. [[CrossRef](#)]
20. Ivanova, V.; Vasilev, P.; Stoianov, I.; Andreev, R.; Boneva, A. Design of a Multifunctional Operating Station Based on Augmented Reality (MOSAR). *Cybern. Inf. Technol.* **2021**, *21*, 119–136. [[CrossRef](#)]
21. Lee, R.S.; Lin, Y.H. Development of universal environment for constructing 5-axis virtual machine tool based on modified D-H notation and OpenGL. *Robot. Comput. Integr. Manuf.* **2010**, *26*, 253–262. [[CrossRef](#)]
22. Wang, H.; Lu, X.; Cui, W.; Zhang, Z.; Li, Y.; Sheng, C. General inverse solution of six-degrees-of-freedom serial robots based on the product of exponentials model. *Assem. Autom.* **2018**, *38*, 361–367. [[CrossRef](#)]
23. You, W.S.; Lee, Y.H.; Oh, H.S.; Kang, G.; Choi, H.R. Design of a 3D-printable, robust anthropomorphic robot hand including intermetacarpal joints. *Intell. Serv. Robot.* **2019**, *12*, 1–16. [[CrossRef](#)]
24. Fusi, L.; Farina, A. Flow of a Bingham fluid in a non symmetric inclined channel. *J. Non-Newton. Fluid Mech.* **2016**, *238*, 24–32. [[CrossRef](#)]

**Disclaimer/Publisher’s Note:** The statements, opinions and data contained in all publications are solely those of the individual author(s) and contributor(s) and not of MDPI and/or the editor(s). MDPI and/or the editor(s) disclaim responsibility for any injury to people or property resulting from any ideas, methods, instructions or products referred to in the content.